



Article

Photo-Thermal Tuning of Graphene Oxide Coated Integrated Optical Waveguides

Yang Qu ¹, Yunyi Yang ², Jiayang Wu ^{1,*}, Yuning Zhang ¹, Linnan Jia ¹, Houssein El Dirani ³, Romain Crochemore ⁴, Corrado Sciancalepore ⁵, Pierre Demongodin ⁶, Christian Grillet ⁶, Christelle Monat ⁶, Baohua Jia ^{2,7,*} and David J. Moss ^{1,*}

- ¹ Optical Sciences Center, Swinburne University of Technology, Hawthorn, VIC 3122, Australia; yqu@swin.edu.au (Y.Q.); yuningzhang@swin.edu.au (Y.Z.); ljia@swin.edu.au (L.J.)
- ² Center for Translational Atomaterials, Swinburne University of Technology, Hawthorn, VIC 3122, Australia; yunyiiyang@swin.edu.au
- ³ STMicroelectronics, CEDEX, 38926 Crolles, France; houssein.eldirani@st.com
- ⁴ Minatec, Optics and Photonics Division, CEA-LETI, 38054 Grenoble, France; romain.crochemore@cae.fr
- ⁵ Soitec SA, 38190 Bernin, France; corrado.sciancalepore@soitec.com
- ⁶ Institut des Nanotechnologies de Lyon, UMR CNRS 5270, Ecole Centrale Lyon, 69130 Ecully, France; pierre.demongodin@ec-lyon.fr (P.D.); christian.grillet@ec-lyon.fr (C.G.); christelle.monat@ec-lyon.fr (C.M.)
- ⁷ School of Science, RMIT University, Melbourne, VIC 3001, Australia
- * Correspondence: jiayangwu@swin.edu.au (J.W.); bjia@swin.edu.au (B.J.); dmoss@swin.edu.au (D.J.M.)

Abstract: We experimentally investigate power-sensitive photo-thermal tuning (PTT) of two-dimensional (2D) graphene oxide (GO) films coated on integrated optical waveguides. We measure the light power thresholds for reversible and permanent GO reduction in silicon nitride (SiN) waveguides integrated with one and two layers of GO. For the device with one layer of GO, the power threshold for reversible and permanent GO reduction are ~20 and ~22 dBm, respectively. For the device with two layers of GO, the corresponding results are ~13 and ~18 dBm, respectively. Raman spectra at different positions of a hybrid waveguide with permanently reduced GO are characterized, verifying the inhomogeneous GO reduction along the direction of light propagation through the waveguide. The differences between the PTT induced by a continuous-wave laser and a pulsed laser are also compared, confirming that the PTT mainly depend on the average input power. These results reveal interesting features for 2D GO films coated on integrated optical waveguides, which are of fundamental importance for the control and engineering of GO's properties in hybrid integrated photonic devices.

Keywords: 2D materials; integrated optics; photo-thermal changes; graphene oxide



Citation: Qu, Y.; Yang, Y.; Wu, J.; Zhang, Y.; Jia, L.; El Dirani, H.; Crochemore, R.; Sciancalepore, C.; Demongodin, P.; Grillet, C.; et al. Photo-Thermal Tuning of Graphene Oxide Coated Integrated Optical Waveguides. *Micromachines* **2022**, *13*, 1194. <https://doi.org/10.3390/mi13081194>

Academic Editor: Maurizio Casalino

Received: 24 June 2022

Accepted: 26 July 2022

Published: 28 July 2022

Publisher's Note: MDPI stays neutral with regard to jurisdictional claims in published maps and institutional affiliations.



Copyright: © 2022 by the authors. Licensee MDPI, Basel, Switzerland. This article is an open access article distributed under the terms and conditions of the Creative Commons Attribution (CC BY) license (<https://creativecommons.org/licenses/by/4.0/>).

1. Introduction

Graphene oxide (GO) is a two-dimensional (2D) material that has attracted significant interest because of its many attractive properties such as broadband photoluminescence [1–3], high optical nonlinearity [4–6], strong material anisotropy [7–9], broadband light absorption [10–12], and tunable material properties in wide ranges [13–15]. In addition, with its facile fabrication processes, GO has a strong capability for large-scale and manufacturable on-chip integration [8,16].

The incorporation of GO into integrated photonic devices has led to the birth of GO-based integrated photonics, which has become a very active and fast-growing field [17]. Integrated photonic devices incorporating GO films have been demonstrated for a range of applications, such as light absorbers [10,11,18], optical lenses and imaging devices [16,19,20], polarization-selective devices [8,9], sensors [21–23], and nonlinear optical devices [24–28].

Since GO can be converted to a reduced form with graphene-like properties under strong light irradiation, high temperature, or microwave treatment [29–33], it has long been used as a precursor for the preparation of graphene [17,34,35]. Given the difference between the material properties of GO and reduced GO (rGO) [4,16,36], investigating the

mechanisms and conditions for GO reduction in hybrid integrated photonic devices is of fundamental importance for applying this functional 2D material to integrated photonic devices [17,37].

Previously, we observed power-sensitive photo-thermal changes in GO films coated onto integrated photonic waveguides [24] and ring resonators [38] in connection with nonlinear four-wave mixing experiments. The contribution from the photo-thermal changes to the measurement results is not insignificant. However, so far there has not been an investigation to quantify such an impact. In this paper, we provide a more detailed characterization for such changes arising from a range of effects such as photo-thermal reduction, thermal dissipation, and self-heating in GO layers. We experimentally investigate photo-thermal tuning (PTT) of 2D GO films coated on integrated optical waveguides. We measure the light power thresholds for reversible and permanent GO reduction in silicon nitride (SiN) waveguides integrated with one and two layers of GO. We identify three reduction stages according to whether the changes are reversible or permanent reductions. Raman spectra at different positions of a hybrid waveguide with a permanently reduced GO film are also characterized, showing the inhomogeneous nature of GO reduction in the direction of light propagation through the waveguide. Finally, we compare the PTT induced by a continuous-wave (CW) laser and a pulsed laser with the same average power, and observe negligible difference between them. This confirms that the PTT mainly depends on the average power rather than the peak power of input light. These results reveal interesting features for the reduction of GO induced by photo-thermal changes, which are useful for controlling and engineering GO's material properties in hybrid integrated photonic devices.

2. Device Design and Fabrication

Figure 1a shows a schematic illustration of a GO-coated SiN waveguide with a mono-layer GO film. The bare SiN waveguide has a cross-section of $1.70 \times 0.72 \mu\text{m}$. A complementary metal-oxide-semiconductor (CMOS) compatible crack-free method [39] was utilized to fabricate the uncoated SiN waveguides. First, a two-step deposition of SiN films was achieved via low-pressure chemical vapor deposition (LPCVD) for strain management and crack prevention. Next, 248-nm deep ultraviolet lithography and dry etching based on $\text{CF}_4/\text{CH}_2\text{F}_2/\text{O}_2$ fluorine were used for waveguide patterning. After that, a silica cladding layer was deposited, followed by window opening on it down to the waveguide top surface via lithography and dry etching processes. The window was located near the waveguide input to enable a relatively high optical power injected into the GO coated segment [40]. The length of the opened window was $L_w = 1.4 \text{ mm}$, and the total length of the SiN waveguide was $L = 2 \text{ cm}$. Finally, 2D layered GO films were coated onto the SiN waveguide by using a solution-based method (first proposed in [16]) that enabled transfer-free and layer-by-layer film coating. This method, which is based on film self-assembly via electrostatic forces, has been employed in many previous reports [8,10,11,24,25,38]. As evidenced by the substantial experimental results in the previous papers, the GO films fabricated using this method show a high reproducibility in terms of film properties (e.g., thickness, conductivity, refractive index, light absorption, and third-order optical nonlinearity), together with good morphology and high uniformity across large coated areas. Compared to the cumbersome film transfer processes employed for on-chip integration of 2D materials such as graphene and TMDCs [41–45], this GO coating method is highly scalable, enabling the precise control of the GO layer number (i.e., film thickness), the ability to coat large-area films, and good film attachment onto integrated chips [16,17,46]. A detailed characterization of the thicknesses (i.e., layer numbers) of the as-prepared GO films was reported in [8,16,24,25,38] using atomic force microscopy (AFM), confirming the good morphology and high uniformity of film coating over large areas (e.g., 4-inch silicon wafer). Here, we only took microscope images for the fabricated devices to check whether there was waveguide damage or dust particles. A micrograph of the fabricated device corresponding to Figure 1a is shown in Figure 1b. The GO film coated on the chip surface exhibited good

morphology, high transmittance, and high uniformity. Figure 1c shows a schematic for the cross section of the GO-SiN waveguide in Figure 1a, the corresponding TE mode profile is shown in Figure 1d. The light-matter interaction between the waveguide evanescent field and the GO film can induce power-sensitive photo-thermal changes in the GO film, which has been observed previously [24,37,38]. In this paper, we only investigate PTT induced by the TE polarized light since TE polarization supports the in-plane interaction between the waveguide evanescent field and the 2D GO film, which is much stronger compared to the out-of-plane interaction given the significant anisotropy of 2D GO films [8,41,42,47,48], thus allowing for the excitation of higher levels of photo thermal changes.

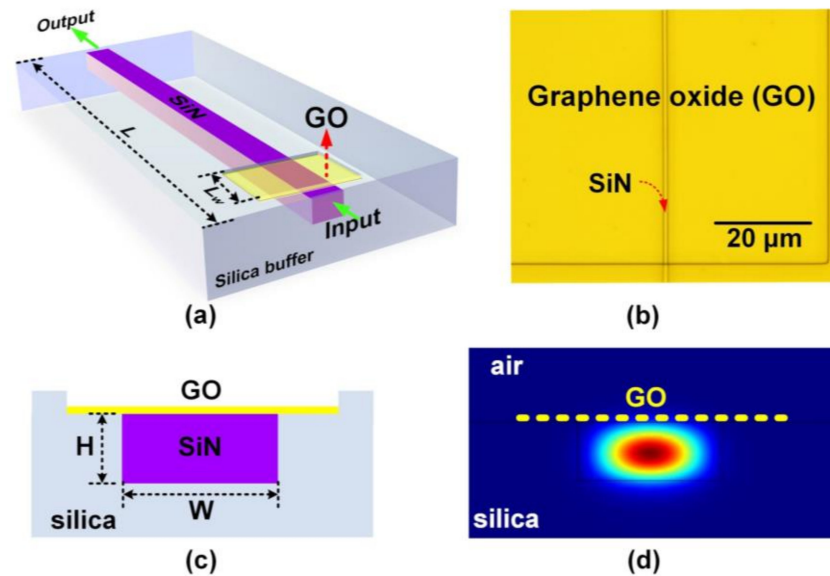


Figure 1. (a) Schematic illustration of a SiN waveguide coated with 1 layer of GO. (b) A micrograph showing the area around the opened window of the fabricated device corresponding to (a). (c) Schematic illustration of the cross-section of the hybrid waveguide. (d) TE mode profile corresponding to (c).

3. Experimental Results

Figure 2 shows the experimental setup for characterizing PTT of GO films coated on integrated optical waveguides. Two CW light sources having different powers were employed. The low power one was used to measure the loss at low powers without measurable photo-thermal changes in the GO films, whereas the high-power one was achieved by amplification with an erbium-doped fiber amplifier (EDFA) to excite the PTT. A pulsed laser source (repetition rate: 60 MHz, pulse width: 3.7 ps) was also employed to compare the level of photo-thermal changes with that induced by the CW light. The wavelengths of both the CW sources and the center wavelength of the picosecond optical pulses were near 1550 nm. Polarization controllers (PCs) were employed to ensure the TE polarization of the input light. An optical isolator was inserted in the high-power light path to prevent the reflected light from damaging the light source. The input laser was split into two beams via a 50:50 beam splitter, with one injecting into the device under test (DUT) and the other sent to an optical power meter (OPM) for monitoring the input power. Lensed fibers were used to butt couple light into and out of the DUT with a coupling loss of ~ 2 dB/facet. A charged-coupled device (CCD) camera was placed above the waveguide to monitor the adjusting of the coupling. Another OPM was employed to measure the output power after passing through the DUT.

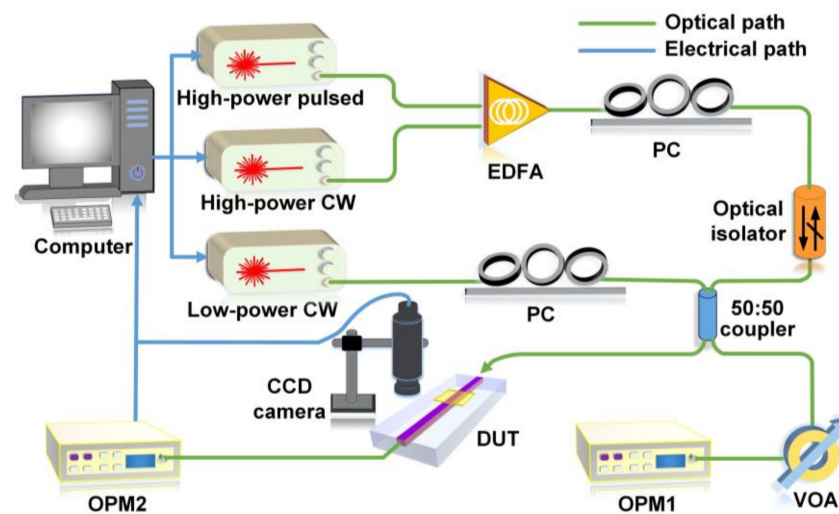


Figure 2. Experimental setup for characterization of PTT of GO-coated integrated waveguides. EDFA: erbium-doped fiber amplifier. PC: polarization controller. DUT: device under test. CCD: charged-coupled device. VOA: variable optical attenuator. OPM: optical power meter.

Figure 3a depicts the measured insertion loss of the integrated waveguide coated with 1 layer of GO versus input CW power. Unless otherwise specified, the input power of CW light or optical pulses in this paper represents the power coupled into the waveguide after subtracting the fiber-to-chip coupling loss. In order to characterize both the reversible and permanent changes of the material properties, after each measurement at a specific input power, we turned off the high-power CW light and remeasured the insertion loss with low-power CW light at 0 dBm. The insertion loss was measured after applying the CW power for about 30 s, which was long enough for the waveguide to reach a steady thermal equilibrium state. The results measured using the high-power and the low-power CW light sources are shown by the red and blue dots, respectively. As can be seen, the evolution of the PTT of the GO film can be divided into three reduction stages. At Stage I, when the input power was below 20 dBm, the insertion loss of the waveguide remained constant despite the increase in input power, reflecting that there was negligible change in the absorption of the GO film and that the light power was not high enough to induce obvious photo-thermal changes. At Stage II starting from 20 dBm, the insertion loss showed a slight but observable increase with the input power, indicating the occurrence of the photo-thermal changes in the GO film. The results measured using low-power CW light after turning off the high-power CW light remained constant. This reflects the fact that there were no permanent changes in the GO films, and the photo-thermal changes at this stage were reversible. These features of the photo-thermal changes in the GO films are consistent with previous reports [24,37,40,42]. For Stage III, when the input power was further increased to above 22 dBm, the results measured using low-power CW light also showed an obvious increase with input power. Since permanently reduced GO films did not show any obvious power dependence [10,11], this reflects the fact that there were permanent changes in the GO films. In addition, the difference between the red dots and their corresponding blue dots indicates that there was still reversibly reduced GO and only part of the GO film was permanently reduced. We infer that there would be a new stage after Stage III at even higher powers, where the difference between the red and blue dots at the same power would vanish due to the full reduction of all the GO films [49,50]. We could not observe this stage in our experiments since we had already applied the maximum experimentally available power to the DUT.

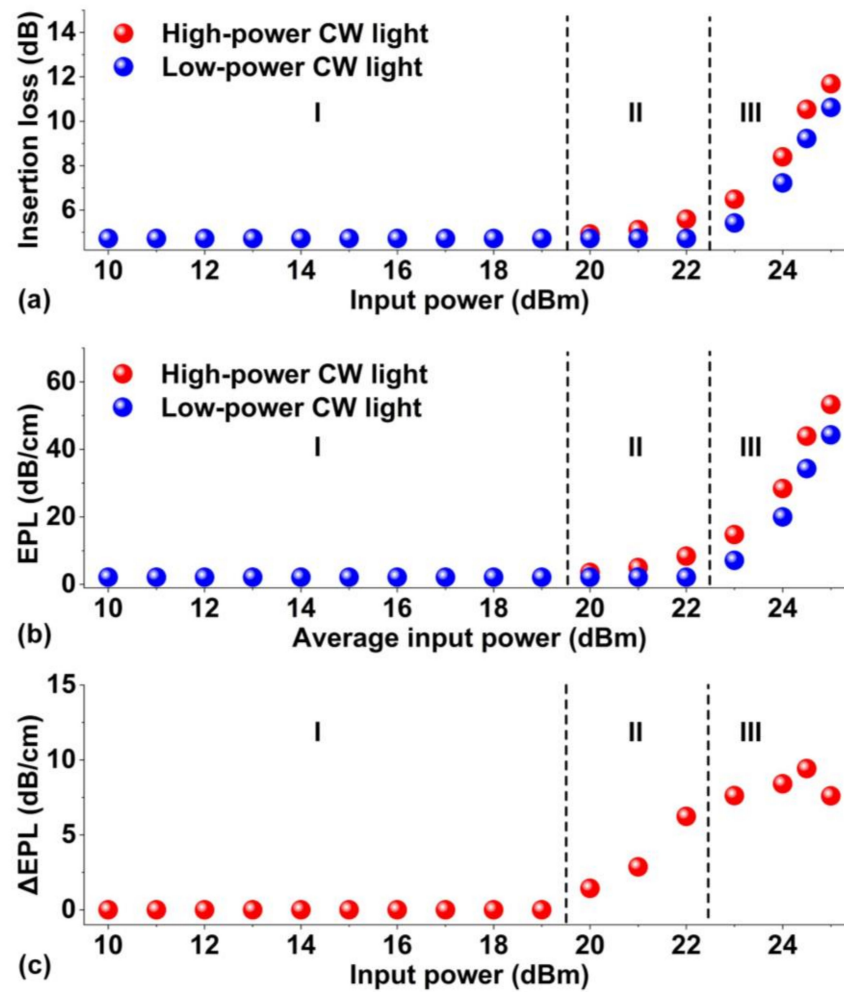


Figure 3. Experimental results for characterizing PTT of the hybrid waveguide coated with 1 layer of GO. (a) Insertion loss of the hybrid waveguide versus the input power of the high-power light source. The red dots show the loss of the high-power CW light source, and the blue dots show the loss measured with a low-power CW light source after exposure at the power level indicated on the X-axis. (b) GO-induced excess propagation loss (EPL) versus input power of the high-power light source. The red and blue dots show the results corresponding to the red and blue dots in (a), respectively. (c) ΔEPL extracted from (b) showing the difference between the red and blue dots. In (a–c), I–III show the three reduction stages during the PTT process.

Figure 3b depicts the GO-induced excess propagation loss (EPL) extracted from Figure 3a. The EPL (dB/cm) is defined as

$$EPL = (IL - IL_0)/L_w \tag{1}$$

where IL is the measured insertion loss of the hybrid waveguide in Figure 3a, IL_0 is the insertion loss of the bare waveguide, and L_w is the GO film length. Figure 3c shows the ΔEPL extracted from Figure 3b, which is defined as the difference between the red and blue dots after exposure by the high-power CW source at the input power indicated on the x-axis. As can be seen, the ΔEPL remained zero at Stage I, and started to increase at Stage II. In Stage III, the ΔEPL first slightly increased and then decreased when the input power was above 24 dBm. This can be attributed to the hybrid nature of GO films at this stage involving the co-existence of permanently and reversibly reduced GO.

The corresponding experimental results for the hybrid waveguide coated with 2 layers of GO are shown in Figure 4. Figure 4a shows the measured insertion loss versus input

CW power. Similar to the results for the device with 1 layer of GO, the evolution of the PTT of the device with 2 layers of GO can also be divided into three reduction stages with increasing input power. Compared to the results in Figure 3a, the power thresholds for Stage II and Stage III were lower, with Stage II starting at 13 dBm and Stage III starting at 18 dBm. This reflects the fact that the power endurance of the film with 2 layers of GO was lower than the film with 1 layer of GO.

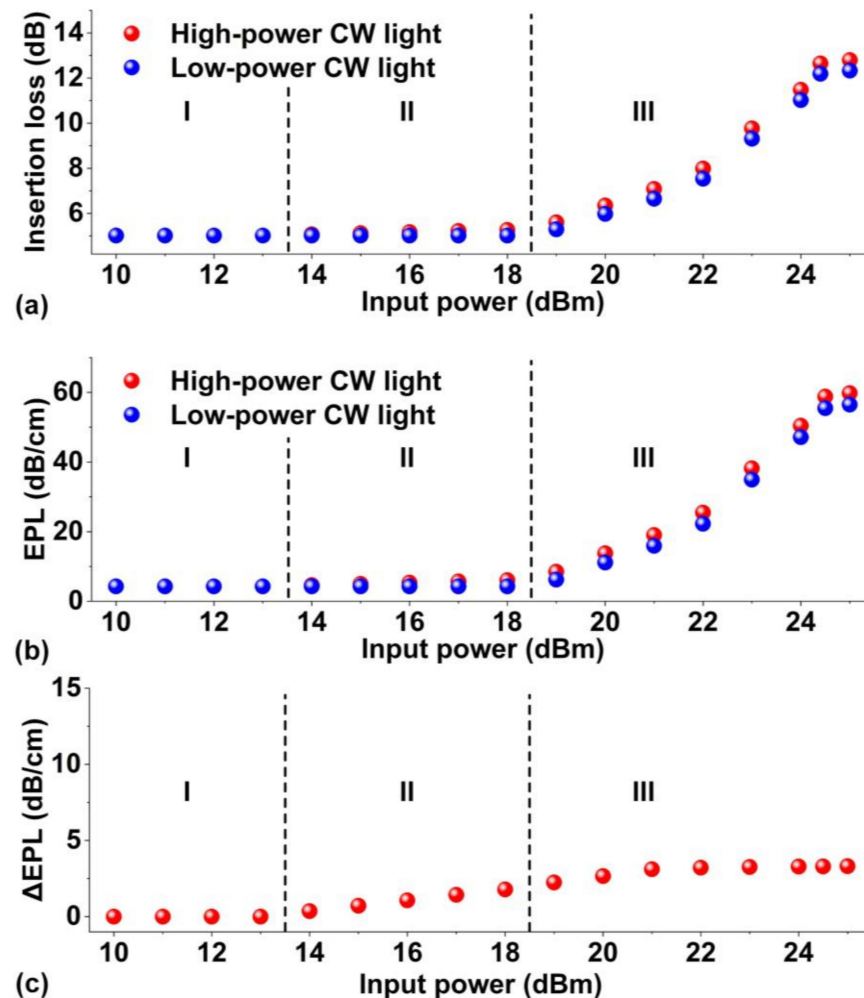


Figure 4. Experimental results for characterizing PTT of the hybrid waveguide coated with 2 layers of GO. (a) Insertion loss of the hybrid waveguide versus the input power of the high-power light source. The red dots show the loss of the high-power CW light source, and the blue dots show the loss measured with a low-power CW light source after exposure at the power level indicated on the X-axis. (b) GO-induced excess propagation loss (EPL) versus input power of the high-power light source. The red and blue dots show the results corresponding to the red and blue dots in (a), respectively. (c) ΔEPL extracted from (b) showing the difference between the red and blue dots. In (a–c), I–III shows the three reduction stages during the PTT process.

Figure 4b shows the GO induced EPL extracted from Figure 4a. Compared to the results in Figure 3b, the EPL here increased more slowly with input power. At Stage I, the excess propagation loss induced in the film with 2 layers of GO is about twice that induced in films with a single layer of GO. However, at Stage II and Stage III, the difference between the EPL induced in 1 and 2 layers of GO became smaller, particularly at higher powers above 20 dBm. This is because the EPL defined in Equation (1) is a parameter averaged over the GO film length, whereas the reduction of GO in practical hybrid waveguides induced by the photo thermal changes is nonuniform, i.e., the GO film at the beginning of

the waveguide is more easily reduced, which absorbs more light power and so protects the GO film following it from being reduced. The film with 2 layers of GO absorbed more light than the film with 1 layer of GO, and so the light transmission was more attenuated over a shorter distance, resulting in a higher proportion of unreduced GO. The loss of the non-reduced 2 layers of GO was lower than the single layer of rGO, thus resulting in a lower *EPL*.

Figure 4c shows the ΔEPL extracted from Figure 4b. Unlike the trend in Figure 3c, the ΔEPL here increases with input power in Stages II and III without showing obvious decrease. This is because for the hybrid waveguide with 2 layers of GO, only a small length of the GO film near the waveguide input was permanently reduced, leaving significant lengths of GO films that were either non-reduced or only reversibly reduced. Although the ΔEPL increased to above zero at relatively low input power for the device with 2 layers of GO, it increased more slowly with input power, with the values at high input powers being smaller than those for the device with 1 layer of GO. This is because for the film with 2 layers of GO, the reversibly reduced GO experienced relatively lower power (14–18 dBm), while the film exposed to higher power was permanently reduced and no longer exhibited ΔEPL . On the other hand, for the single layer GO film, the reversibly reduced GO experienced relatively higher powers (20–22 dBm), thus yielding a higher ΔEPL .

4. Discussion

In Section 3, the inhomogeneous GO reduction along the hybrid waveguides was used to explain several experimental phenomena. To verify the inhomogeneous nature of the GO reduction induced by the photo-thermal changes, we characterized the Raman spectra of two layers of GO coated on an integrated waveguide after applying a maximum input power of 24 dBm. Micro-Raman spectroscopy (inVia Raman microspectrometer, which consisted of a Raman spectrometer integrated with a $100\times$ objective to focus the light beam) with a spot diameter on the order of 10^{-6} m (close to the width of the integrated waveguide) was employed. The laser wavelength was ~ 514 nm. The irradiance laser intensity was on the order of 10^{-1} GW/cm², which was kept the same for all measurements. The results are shown in Figure 5, where representative D and G peaks of GO can be clearly identified. Near the waveguide input, the D and G peaks of the detected Raman signals are relatively small, with a D/G ratio being larger than 1. This is similar to that of rGO [16,51,52], indicating that the GO film here was reduced. In contrast, for positions further away from the waveguide input, the D/G ratio decreased to less than 1, together with an increased intensity for the detected Raman signal. These characteristics show agreement with Raman spectra of GO having fewer defects [13,53,54] and reflect the fact that the GO away from the waveguide input was reduced less. According to our previous measurements [16], only fully reduced GO (with its material properties close to graphene) shows an obvious 2D peak in the Raman spectrum, whereas GO and partially reduced GO do not show obvious 2D peaks. For the Raman spectra in Figure 5, no obvious 2D peaks were observed. Therefore, we infer that the GO film coated on the integrated waveguide was not fully reduced despite the fact that there were permanent changes in its properties.

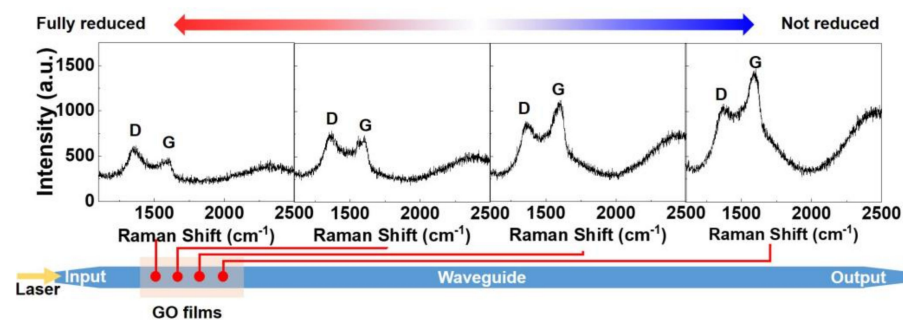


Figure 5. Raman spectra of 2 layers of GO coated on an integrated waveguide after applying an input CW power of 24 dBm.

To compare the PTT induced by CW light versus optical pulses, we measured the *EPLs* of the hybrid waveguides with a single GO layer for both CW light and optical pulses having the same average power. The results are shown in Figure 6. The optical pulses had a repetition rate of ~60 MHz and a pulse width of ~3.7 ps, which corresponded to a peak power 4×10^3 times higher than the CW light with the same average power. As can be seen, both the CW light and the optical pulses induced measurable *EPLs* at high average input powers. The small difference between them indicates that the *EPL* was mainly a function of the average power rather than peak power. This is in agreement with observations in GO films arising from photo-thermal processes in previous works [24,37,38], and further confirms the existence of the photo thermal changes. In contrast, the changes induced by ultrafast nonlinear optical processes such as four-wave mixing, two-photon absorption, and saturable absorption are dependent on the peak input light power [40,55–59]. The slightly lower *EPL* induced by optical pulses compared to CW light can be attributed to saturable absorption in the GO films caused by the high peak powers, which was also observed in previous works [25,28,39]. We also measured permanent *EPLs* at low-power CW light (0 dBm) after turning off the high-power CW light and optical pulses. The permanent *EPLs* induced by the CW and optical pulses showed negligible difference, reflecting the fact that the permanent reduction of GO was mainly induced by the photo-thermal changes. Since the pulsed laser source used in our measurements only had fixed pulse width and period, we did not investigate the photo-thermal changes induced by optical pulses with different widths and periods, which is interesting and could be the subject of future work.

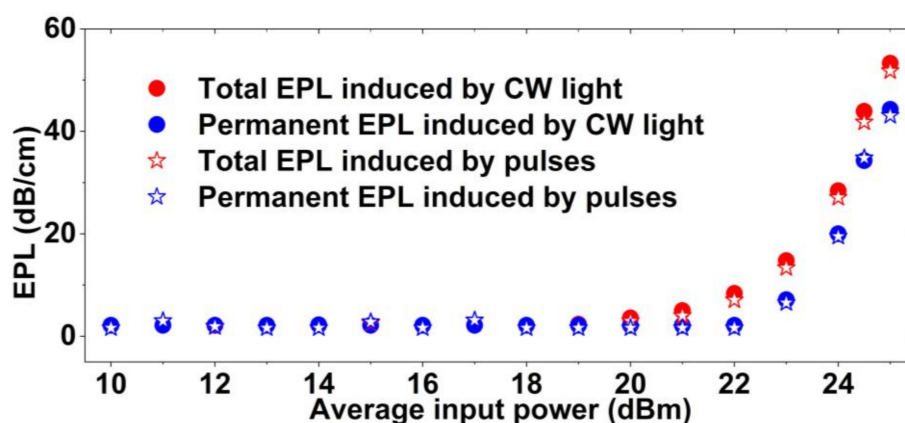


Figure 6. Experimental results of the total and permanent *EPL* induced by a CW light and optical pulses versus average input power for the hybrid waveguides coated with 1 layer of GO.

5. Conclusions

We present detailed investigations of the PTT of GO films coated on integrated optical waveguides. Reversible and permanent GO reduction is observed by applying different CW laser powers to the devices with one and two layers of GO. The corresponding power thresholds are measured, with three reduction stages being identified. For the device with one layer of GO, the power threshold for reversible and permanent GO reduction are ~20 and ~22 dBm, respectively. For the device with two layers of GO, the corresponding results are ~13 and ~18 dBm, respectively. The Raman spectra at different positions of a hybrid waveguide with a permanently reduced GO film are characterized, which verifies the inhomogeneity of GO reduction. The photo-thermal changes induced by CW light and optical pulses with the same average power are also compared, which show negligible difference and confirms that the PTT mainly depends on the average input power. These results are useful for controlling and engineering the material properties of GO in hybrid integrated photonic devices.

Author Contributions: Conceptualization, methodology, J.W. and Y.Q.; silicon nitride device design and fabrication, H.E.D., R.C., P.D., C.S., C.G. and C.M.; GO film coating and material characterization,

Y.Y., Y.Z. and L.J.; writing—original draft preparation, Y.Q. and J.W.; writing—review and editing, J.W., Y.Q. and D.J.M.; supervision, J.W., B.J. and D.J.M. All authors have read and agreed to the published version of the manuscript.

Funding: This work was supported by the Australian Research Council Discovery Projects Programs (No. DP150102972 and DP190103186), the Swinburne ECR-SUPRA program (Swinburne Research), the Industrial Transformation Training Centers scheme (Grant No. IC180100005), the Beijing Natural Science Foundation (No. Z180007), the Agence Nationale de la Recherche (ANR) (Grant No. MIRSiCOMB, ANR-17-CE24-0028), and the H2020 European Research Council (ERC) (Grant No. GRAPHICS, 648546). The work of Christian Grillet and Christelle Monat was supported by the International Associated Laboratory in Photonics between France and Australia (LIA ALPhFA).

Acknowledgments: The authors acknowledge the Swinburne Nano Lab for the support in device fabrication and characterization.

Conflicts of Interest: The authors declare no conflict of interest.

References

1. Chien, C.-T.; Li, S.-S.; Lai, W.-J.; Yeh, Y.-C.; Chen, H.-A.; Chen, I.-S.; Chen, L.-C.; Chen, K.-H.; Nemoto, T.; Isoda, S.; et al. Tunable photoluminescence from graphene oxide. *Angew. Chem. Int.* **2012**, *51*, 6662–6666. [[CrossRef](#)] [[PubMed](#)]
2. Cushing, S.K.; Li, M.; Huang, F.; Wu, N. Origin of strong excitation wavelength dependent fluorescence of graphene oxide. *ACS Nano* **2014**, *8*, 1002–1013. [[CrossRef](#)] [[PubMed](#)]
3. Eda, G.; Lin, Y.Y.; Mattevi, C.; Yamaguchi, H.; Chen, H.A.; Chen, I.S.; Chen, C.W.; Chhowalla, M. Blue photoluminescence from chemically derived graphene oxide. *Adv. Mater.* **2010**, *22*, 505–509. [[CrossRef](#)] [[PubMed](#)]
4. Zheng, X.R.; Jia, B.H.; Chen, X.; Gu, M. In situ third-order nonlinear responses during laser reduction of graphene oxide thin films towards on-chip nonlinear photonic devices. *Adv. Mater.* **2014**, *26*, 2699–2703. [[CrossRef](#)]
5. Russier-Antoine, I.; Fakhouri, H.; Basu, S.; Bertorelle, F.; Dugourd, P.; Brevet, P.-F.; Velayudhan, P.; Thomas, S.; Kalarikkal, N.; Antoine, R. Second harmonic scattering from mass characterized 2D graphene oxide sheets. *Chem. Commun.* **2020**, *56*, 3859–3862. [[CrossRef](#)]
6. Liu, Z.-B.; Zhao, X.; Zhang, X.-L.; Yan, X.-Q.; Wu, Y.-P.; Chen, Y.-S.; Tian, J.-G. Ultrafast dynamics and nonlinear optical responses from sp^2 - and sp^3 -hybridized domains in graphene oxide. *J. Phys. Chem. Lett.* **2011**, *2*, 1972–1977. [[CrossRef](#)]
7. Lim, W.H.; Yap, Y.K.; Chong, W.Y.; Pua, C.H.; Huang, N.M.; De La Rue, R.M.; Ahmad, H. Graphene oxide-based waveguide polariser: From thin film to quasi-bulk. *Opt. Express* **2014**, *22*, 11090–11098. [[CrossRef](#)]
8. Wu, J.Y.; Yang, Y.Y.; Qu, Y.; Xu, X.Y.; Liang, Y.; Chu, S.T.; Little, B.E.; Morandotti, R.; Jia, B.H.; Moss, D.J. Graphene oxide waveguide and micro-ring resonator polarizers. *Laser Photonics Rev.* **2019**, *13*, 1900056. [[CrossRef](#)]
9. Chong, W.; Gan, S.; Lai, C.; Chong, W.; Choi, D.; Madden, S.; De La Rue, R.; Ahmad, H. Configurable TE- and TM-pass graphene oxide-coated waveguide polarizer. *IEEE Photonics Technol. Lett.* **2020**, *32*, 627–630. [[CrossRef](#)]
10. Lin, H.; Sturmberg, B.C.P.; Lin, K.-T.; Yang, Y.; Zheng, X.; Chong, T.K.; de Sterke, C.M.; Jia, B. A 90-nm-thick graphene metamaterial for strong and extremely broadband absorption of unpolarized light. *Nat. Photonics* **2019**, *13*, 270–276. [[CrossRef](#)]
11. Lin, K.-T.; Lin, H.; Yang, T.; Jia, B. Structured graphene metamaterial selective absorbers for high efficiency and omnidirectional solar thermal energy conversion. *Nat. Commun.* **2020**, *11*, 1389. [[CrossRef](#)]
12. Yin, Z.; Zhu, J.; He, Q.; Cao, X.; Tan, C.; Chen, H.; Yan, Q.; Zhang, H. Graphene-based materials for solar cell applications. *Adv. Energy Mater.* **2014**, *4*, 1300574. [[CrossRef](#)]
13. Loh, K.P.; Bao, Q.; Eda, G.; Chhowalla, M. Graphene oxide as a chemically tunable platform for optical applications. *Nat. Chem.* **2010**, *2*, 1015–1024. [[CrossRef](#)]
14. El-Kady, M.F.; Strong, V.; Dubin, S.; Kaner, R.B. Laser scribing of high-performance and flexible graphene-based electrochemical capacitors. *Science* **2012**, *335*, 1326–1330. [[CrossRef](#)]
15. Gao, W.; Singh, N.; Song, L.; Liu, Z.; Reddy, A.L.M.; Ci, L.; Vajtai, R.; Zhang, Q.; Wei, B.; Ajayan, P.M. Direct laser writing of micro-supercapacitors on hydrated graphite oxide films. *Nat. Nanotechnol.* **2011**, *6*, 496–500. [[CrossRef](#)]
16. Yang, Y.; Lin, H.; Zhang, B.Y.; Zhang, Y.; Zheng, X.; Yu, A.; Hong, M.; Jia, B. Graphene-based multilayered metamaterials with phototunable architecture for on-chip photonic devices. *ACS Photonics* **2019**, *6*, 1033–1040. [[CrossRef](#)]
17. Wu, J.; Jia, L.; Zhang, Y.; Qu, Y.; Jia, B.; Moss, D.J. Graphene oxide for integrated photonics and flat optics. *Adv. Mater.* **2021**, *33*, 2006415. [[CrossRef](#)]
18. Larsen, L.J.; Shearer, C.J.; Ellis, A.V.; Shapter, J.G. Optimization and doping of reduced graphene oxide–silicon solar cells. *J. Phys. Chem. C* **2016**, *120*, 15648–15656. [[CrossRef](#)]
19. Zheng, X.; Jia, B.; Lin, H.; Qiu, L.; Li, D.; Gu, M. Highly efficient and ultra-broadband graphene oxide ultrathin lenses with three-dimensional subwavelength focusing. *Nat. Commun.* **2015**, *6*, 8433. [[CrossRef](#)]
20. Huang, C.; Zhang, X.; Li, Y.; Yang, X. Hyaluronic acid and graphene oxide loaded silicon contact lens for corneal epithelial healing. *J. Biomater. Sci. Polym. Ed.* **2021**, *32*, 372–384. [[CrossRef](#)]

21. Leo Tsui, H.C.; Alsalman, O.; Mao, B.; Alodhayb, A.; Albrithen, H.; Knights, A.P.; Halsall, M.P.; Crowe, I.F. Graphene oxide integrated silicon photonics for detection of vapour phase volatile organic compounds. *Sci. Rep.* **2020**, *10*, 9592. [[CrossRef](#)]
22. He, S.; Song, B.; Li, D.; Zhu, C.; Qi, W.; Wen, Y.; Wang, L.; Song, S.; Fang, H.; Fan, C. A graphene nanoprobe for rapid, sensitive, and multicolor fluorescent DNA analysis. *Adv. Funct. Mater.* **2010**, *20*, 453–459. [[CrossRef](#)]
23. Morales-Narváez, E.; Merkoçi, A. Graphene oxide as an optical biosensing platform. *Adv. Mater.* **2012**, *24*, 3298–3308. [[CrossRef](#)]
24. Qu, Y.; Wu, J.; Yang, Y.; Zhang, Y.; Liang, Y.; El Dirani, H.; Crochemore, R.; Demongodin, P.; Sciancalepore, C.; Grillet, C.; et al. Enhanced four-wave mixing in silicon nitride waveguides integrated with 2D layered graphene oxide films. *Adv. Opt. Mater.* **2020**, *8*, 2001048. [[CrossRef](#)]
25. Zhang, Y.; Wu, J.; Yang, Y.; Qu, Y.; Jia, L.; Moein, T.; Jia, B.; Moss, D.J. Enhanced Kerr nonlinearity and nonlinear figure of merit in silicon nanowires integrated with 2D graphene oxide films. *ACS Appl. Mater. Interfaces* **2020**, *12*, 33094–33103. [[CrossRef](#)]
26. Zhang, Y.; Wu, J.; Qu, Y.; Jia, L.; Jia, B.; Moss, D.J. Optimizing the Kerr nonlinear optical performance of silicon waveguides integrated with 2D graphene oxide films. *J. Lightwave Technol.* **2021**, *39*, 4671–4683. [[CrossRef](#)]
27. Zhang, Y.; Wu, J.; Yang, Y.; Qu, Y.; Jia, L.; Jia, B.; Moss, D.J. Enhanced spectral broadening of femtosecond optical pulses in silicon nanowires integrated with 2D graphene oxide films. *Micromachines* **2022**, *13*, 756. [[CrossRef](#)]
28. Zhang, Y.; Wu, J.; Yang, Y.; Qu, Y.; Dirani, H.E.; Crochemore, R.; Sciancalepore, C.; Demongodin, P.; Grillet, C.; Monat, C.; et al. Enhanced self-phase modulation in silicon nitride waveguides integrated with 2D graphene oxide films. *IEEE J. Sel. Top. Quant.* **2022**. [[CrossRef](#)]
29. Zhang, Y.-L.; Guo, L.; Xia, H.; Chen, Q.-D.; Feng, J.; Sun, H.-B. Photoreduction of graphene oxides: Methods, properties, and applications. *Adv. Opt. Mater.* **2014**, *2*, 10–28. [[CrossRef](#)]
30. Compton, O.C.; Nguyen, S.T. Graphene oxide, highly reduced graphene oxide, and graphene: Versatile building blocks for carbon-based materials. *Small* **2010**, *6*, 711–723. [[CrossRef](#)]
31. Chen, W.; Yan, L.; Bangal, P.R. Preparation of graphene by the rapid and mild thermal reduction of graphene oxide induced by microwaves. *Carbon* **2010**, *48*, 1146–1152. [[CrossRef](#)]
32. Wei, Z.; Wang, D.; Kim, S.; Kim, S.-Y.; Hu, Y.; Yakes, M.K.; Laracuenta, A.R.; Dai, Z.; Marder, S.R.; Berger, C. Nanoscale tunable reduction of graphene oxide for graphene electronics. *Science* **2010**, *328*, 1373–1376. [[CrossRef](#)] [[PubMed](#)]
33. Voiry, D.; Yang, J.; Kupferberg, J.; Fullon, R.; Lee, C.; Jeong, H.Y.; Shin, H.S.; Chhowalla, M. High-quality graphene via microwave reduction of solution-exfoliated graphene oxide. *Science* **2016**, *353*, 1413–1416. [[CrossRef](#)] [[PubMed](#)]
34. Zhu, Y.; Murali, S.; Cai, W.; Li, X.; Suk, J.W.; Potts, J.R.; Ruoff, R.S. Graphene and graphene oxide: Synthesis, properties, and applications. *Adv. Mater.* **2010**, *22*, 3906–3924. [[CrossRef](#)]
35. Brisebois, P.P.; Sijaj, M. Harvesting graphene oxide—Years 1859 to 2019: A review of its structure, synthesis, properties and exfoliation. *J. Mater. Chem. C* **2020**, *8*, 1517–1547. [[CrossRef](#)]
36. Pei, S.; Cheng, H.-M. The reduction of graphene oxide. *Carbon* **2012**, *50*, 3210–3228. [[CrossRef](#)]
37. Chong, W.Y.; Lim, W.H.; Yap, Y.K.; Lai, C.K.; De La Rue, R.M.; Ahmad, H. Photo-induced reduction of graphene oxide coating on optical waveguide and consequent optical intermodulation. *Sci. Rep.* **2016**, *6*, 23813. [[CrossRef](#)]
38. Wu, J.; Yang, Y.; Qu, Y.; Jia, L.; Zhang, Y.; Xu, X.; Chu, S.T.; Little, B.E.; Morandotti, R.; Jia, B.; et al. 2D Layered graphene oxide films integrated with micro-ring resonators for enhanced nonlinear optics. *Small* **2020**, *16*, 1906563. [[CrossRef](#)]
39. Demongodin, P.; El Dirani, H.; Lhuillier, J.; Crochemore, R.; Kemiche, M.; Wood, T.; Callard, S.; Rojo-Romeo, P.; Sciancalepore, C.; Grillet, C.; et al. Ultrafast saturable absorption dynamics in hybrid graphene/Si₃N₄ waveguides. *APL Photonics* **2019**, *4*, 076102. [[CrossRef](#)]
40. Qu, Y.; Wu, J.; Zhang, Y.; Jia, L.; Liang, Y.; Jia, B.; Moss, D.J. Analysis of four-wave mixing in silicon nitride waveguides integrated with 2D layered graphene oxide films. *J. Lightwave Technol.* **2021**, *39*, 2902–2910. [[CrossRef](#)]
41. Feng, Q.; Cong, H.; Zhang, B.; Wei, W.; Liang, Y.; Fang, S.; Wang, T.; Zhang, J. Enhanced optical Kerr nonlinearity of graphene/Si hybrid waveguide. *Appl. Phys. Lett.* **2019**, *114*, 071104. [[CrossRef](#)]
42. Liu, L.; Xu, K.; Wan, X.; Xu, J.; Wong, C.Y.; Tsang, H.K. Enhanced optical Kerr nonlinearity of MoS₂ on silicon waveguides. *Photonics Res.* **2015**, *3*, 206–209. [[CrossRef](#)]
43. Liu, M.; Yin, X.; Ulin-Avila, E.; Geng, B.; Zentgraf, T.; Ju, L.; Wang, F.; Zhang, X. A graphene-based broadband optical modulator. *Nature* **2011**, *474*, 64–67. [[CrossRef](#)]
44. Phare, C.T.; Daniel Lee, Y.-H.; Cardenas, J.; Lipson, M. Graphene electro-optic modulator with 30 GHz bandwidth. *Nat. Photonics* **2015**, *9*, 511–514. [[CrossRef](#)]
45. Sorianello, V.; Midrio, M.; Contestabile, G.; Asselberghs, I.; Van Campenhout, J.; Huyghebaert, C.; Goykhman, I.; Ott, A.; Ferrari, A.; Romagnoli, M. Graphene–silicon phase modulators with gigahertz bandwidth. *Nat. Photonics* **2018**, *12*, 40–44. [[CrossRef](#)]
46. Jia, L.; Wu, J.; Zhang, Y.; Qu, Y.; Jia, B.; Chen, Z.; Moss, D.J. Fabrication technologies for the on-chip integration of 2D materials. *Small Methods* **2022**, *6*, 2101435. [[CrossRef](#)]
47. Gu, T.; Petrone, N.; McMillan, J.F.; van der Zande, A.; Yu, M.; Lo, G.Q.; Kwong, D.L.; Hone, J.; Wong, C.W. Regenerative oscillation and four-wave mixing in graphene optoelectronics. *Nat. Photonics* **2012**, *6*, 554–559. [[CrossRef](#)]
48. Ji, M.; Cai, H.; Deng, L.; Huang, Y.; Huang, Q.; Xia, J.; Li, Z.; Yu, J.; Wang, Y. Enhanced parametric frequency conversion in a compact silicon-graphene microring resonator. *Opt. Express* **2015**, *23*, 18679–18685. [[CrossRef](#)]
49. Seo, S.; Yoon, Y.; Lee, J.; Park, Y.; Lee, H. Nitrogen-doped partially reduced graphene oxide rewritable nonvolatile memory. *ACS Nano* **2013**, *7*, 3607–3615. [[CrossRef](#)]

50. Liu, X.; Hao, Y.; Shu, J.; Sari, H.M.K.; Lin, L.; Kou, H.; Li, J.; Liu, W.; Yan, B.; Li, D. Nitrogen/sulfur dual-doping of reduced graphene oxide harvesting hollow ZnSnS₃ nano-microcubes with superior sodium storage. *Nano Energy* **2019**, *57*, 414–423. [[CrossRef](#)]
51. Eigler, S.; Dotzer, C.; Hirsch, A. Visualization of defect densities in reduced graphene oxide. *Carbon* **2012**, *50*, 3666–3673. [[CrossRef](#)]
52. Luo, D.; Zhang, G.; Liu, J.; Sun, X. Evaluation criteria for reduced graphene oxide. *J. Phys. Chem. C* **2011**, *115*, 11327–11335. [[CrossRef](#)]
53. López, V.; Sundaram, R.S.; Gómez-Navarro, C.; Olea, D.; Burghard, M.; Gómez-Herrero, J.; Zamora, F.; Kern, K. Chemical vapor deposition repair of graphene oxide: A route to highly-conductive graphene monolayers. *Adv. Mater.* **2009**, *21*, 4683–4686. [[CrossRef](#)]
54. Claramunt, S.; Varea, A.; Lopez-Diaz, D.; Velázquez, M.M.; Cornet, A.; Cirera, A. The importance of interbands on the interpretation of the Raman spectrum of graphene oxide. *J. Phys. Chem. C* **2015**, *119*, 10123–10129. [[CrossRef](#)]
55. Jiang, T.; Kravtsov, V.; Tokman, M.; Belyanin, A.; Raschke, M.B. Ultrafast coherent nonlinear nanooptics and nanoimaging of graphene. *Nat. Nanotechnol.* **2019**, *14*, 838–843. [[CrossRef](#)]
56. Zhang, Y.; Wu, J.; Qu, Y.; Jia, L.; Jia, B.; Moss, D.J. Design and optimization of four-wave mixing in microring resonators integrated with 2D graphene oxide films. *J. Lightwave Technol.* **2021**, *39*, 6553–6562. [[CrossRef](#)]
57. Koos, C.; Vorreau, P.; Vallaitis, T.; Dumon, P.; Bogaerts, W.; Baets, R.; Esembeson, B.; Biaggio, I.; Michinobu, T.; Diederich, F.; et al. All-optical high-speed signal processing with silicon-organic hybrid slot waveguides. *Nat. Photonics* **2009**, *3*, 216–219. [[CrossRef](#)]
58. Bao, Q.; Zhang, H.; Wang, Y.; Ni, Z.; Yan, Y.; Shen, Z.X.; Loh, K.P.; Tang, D.Y. Atomic-layer graphene as a saturable absorber for ultrafast pulsed lasers. *Adv. Funct. Mater.* **2009**, *19*, 3077–3083. [[CrossRef](#)]
59. Li, W.; Chen, B.; Meng, C.; Fang, W.; Xiao, Y.; Li, X.; Hu, Z.; Xu, Y.; Tong, L.; Wang, H.; et al. Ultrafast all-optical graphene modulator. *Nano Lett.* **2014**, *14*, 955–959. [[CrossRef](#)]